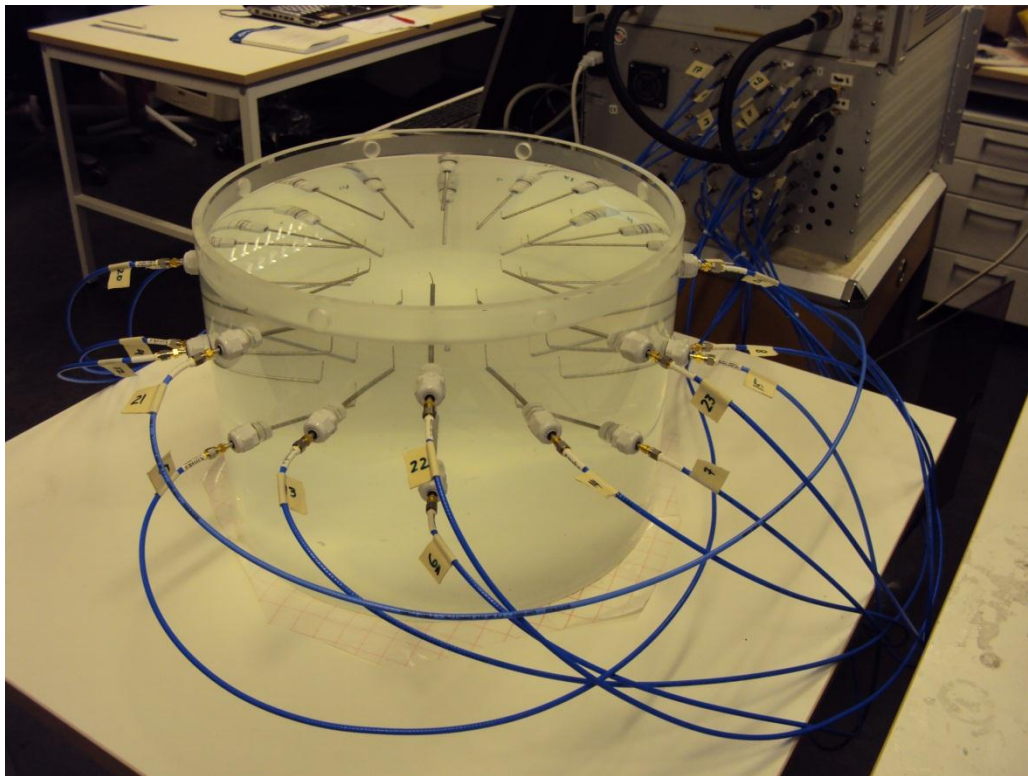


CHALMERS



3-D Microwave Tomography

Microwave Measurements, Image Reconstruction and FDTD modelling

Master of Science Thesis

ADNAN SAEED

Department of Signals and System

CHALMERS UNIVERSITY OF TECHNOLOGY

Gothenburg, Sweden, 2011

Report No. EX098/2011

3-D Microwave Tomography
Image Reconstructon and FDTD modelling

© Adnan Saeed, 2011

Master's Thesis 2011:NN

Department of Signals and Systems
Chalmers University of Technology
SE-41296 Göteborg
Sweden
Telephone +46-(0)31 772 1000

Cover:

The cover shows the protoype developed for Breast cancer imaging. Tank with twenty-four antennas placed cylindricaly in three layers.

Department of Signals and Systems
Göteborg, Sweden 2011

Abstract

This work aims to extend the current development of the equipment for constructing three dimensional images for breast cancer detection. Breast cancer being one of the most common types still requires accurate and cost effective methods for early detection. Microwave tomography for breast cancer detection shows promising results due the fact that there is high contrast ratio between tumour and healthy tissue. Moreover this method is non destructive, radiations are non-ionizing and the procedure is painless for the patient.

Twenty four monopole antennas laid in a cylindrical pattern in a tank filled with water are used for microwave measurements. The phantoms of breasts are prepared and placed within the antenna domain. FDTD based minimization inversion algorithm developed by A.Fhager [1] is used for image reconstruction. A multi-grid approach was implemented in the image reconstruction for a better resolution. The permittivity was well constructed for one object, two objects and was also satisfactory for the constructed breast phantom. The conductivity was not well constructed.

Key words: 3-D Microwave tomography, Antenna Modelling, FDTD, Mammography, Image reconstruction

Acknowledgements

My most humble and sincere thanks to Allah Almighty, with his divine grace and help I was able to complete my work. May Allah help us to perform our duties, to strengthen us on the right path and to guide us towards all that will bring good to us. My deepest gratitude to my supervisor Andreas Fhager, without his help and guidance it would not have been possible for me to complete this work. My parents and family especially my mother, who are a support in every exam of my life. Last but not the least my friends Ashar, Atif, Danial, Saad and Tayyab, having them in my company was one of the best experiences of my life.

The computations were performed on C3SE, Chalmers computing resources.

Contents

1. Introduction	1
2. Microwaves and Tomography	2
Breast Cancer and Microwaves.....	2
Dielectric Properties.....	3
1.1.1. Complex Permittivity	4
1.1.2. Conductivity	4
1.1.3. Biological Tissue Dielectric Properties.....	5
Dispersive response	5
1.1.4. α Dispersion.....	6
1.1.5. β Dispersion.....	6
1.1.6. γ Dispersion	7
DiElectric Model and Debye Equation	7
1.1.7. Maxwell equations.....	7
3. The Experimental Setup	9
Physical Parameters Summary	10
Simulated Parameters Summary	13
Up gradation of Existing Prototype	13
4. The FDTD Modelling.....	14
Image Reconstruction.....	14
FDTD Modelling	15
Antenna Modelling.....	16
Measured Antenna Data vs Simulated Data.....	18
Water Tank Modelling	20
Multi-Grid Approach	21
5. Results and Discussion.....	22
Measured Permittivity	22
One Acrylic Cylinder.....	23
5.1.1. Permittivity	23
5.1.2. Conductivity	24

Two Acrylic Cylinders	26
5.2.1. Permittivity	26
5.2.2. Conductivity	27
Vegetable Oil Cylinder	28
5.3.1. Permittivity	28
5.3.2. Conductivity	30
Ethanol Cylinder	33
5.4.3. Permittivity	33
6. Conclusions and Future Work	35
Bibliography	37

List of Figures

Figure 2-2: Frequency dependence of Permittivity, Literature values by Andreas Fhager, [1].	5
Figure 2-3: Frequency dependence of Conductivity, Literature values by Andreas Fhager, [1].	6
Figure 3-1: Scattering parameters for a Two-Port network	9
Figure 3-2: Antenna Length Measurement	10
Figure 3-3: Length Comparison, Cup, Acrylic Cylinder and Metal Screw	11
Figure 3-4: Top view, Measurement tank filled with water	12
Figure 3-5: Side View, Measurement System connected to a PNA	12
Figure 4-1: Time Stepping Electric and Magnetic field	16
Figure 4-2: The Yee Lattice	16
Figure 4-3: FDTD Modelled Antenna	17
Figure 4-4: Antenna locations in a 3D-Grid used in Simulation	18
Figure 4-5: S11 parameter plot at different Antenna Lengths	19
Figure 14-6: One mm Resolution Grid with Antennas	21
Figure 5-1: Measured Permittivity	22
Figure 5-3: Simulation Single Acrylic Cylinder, Permittivity	23
Figure 5-8: Actual Model Two Acrylic Cylinders, Permittivity	26
Figure 5-10: Actual Model Two Acrylic Cylinders, Conductivity	27
Figure 5-11: Measured Two Acrylic Cylinders, Conductivity	27

1. Introduction

Use of microwaves for radio communication purposes can be traced as early as 1950's. Back then, *microwave radio relay links* were used to carry long distance calls and frequency division multiplexing was used to send up to 5400 telephone channels on each microwave radio channel [10]. Gradually hard wired telephony was replaced by wireless telephony. Now a day's it's hard to find a wireless communication device without using microwaves as a carrier to transmit and receive data. GSM, Wi-Max, Bluetooth, WLAN and other protocols use this band. Among some of the reasons for its global success were that microwaves are easier to control. Small antennas could direct the waves really well and can be confined to a narrow beam width, thus covering larger distances and making it vulnerable for being intercepted. It has also been used in radars for detection and speed measurements of remote objects. The use in radio astronomy is also seen as naturally occurring microwave radiations from the deep space are observed. In the current days Navigation Systems such as in GPS and GLONASS microwave band is used to broadcast navigation signals. Microwaves are also used in ovens for heating drying and curing products.

Microwave imaging for biological tissues was successful when Jacobi and Hast [2] developed an antenna system and imaged a kidney. This technique takes into account the electromagnetic response of different materials for identifying its characteristics. These electromagnetic properties are discussed in detail latter in the report. In short, scattered electric field is measured whenever the transmitted waves interact with an object.

2. Microwaves and Tomography

Tomography is an imaging technique in which different slices of the object are constructed by transmission or reflection data. This data is obtained by illuminating the object by any penetrating wave. In microwave tomography these waves are *microwaves*. They are electromagnetic waves with frequency between 300 MHz to 300 GHz. In our developed prototype object is illuminated over a frequency band of 300 MHz to 3 GHz. Within this range high contrast is reported in the literature between healthy and tumorous tissue.

Today the routine exam for breast cancer detection is X-ray Mammography. Low energy X-rays are used as doses of ionized radiation to create images. The exposure of radiation with mammography is a potential risk even if the radiation dose is kept low there is still a possibility of radiation induced cancer.

Another limitation of this technique is false negative this is a rate of missed tumours. Accurate data regarding the number of false negatives are very difficult to obtain, according to *Politics of Cancer*, in women ages 40 to 49, one in four instances of cancer is missed at each mammography [3]. Difficulty arises when the breasts are radiographically dense and comparatively there is a low contrast between tumour and surrounding tissue in this technique. The process of examination can also be painful for the patient as imaging with this technique requires sufficient breast compression

Breast Cancer and Microwaves

The breast is a mass of glandular, fatty, and fibrous tissues. Breast cancer is a cancer originating from breast tissue, most commonly from the inner lining of milk ducts or the lobules that supply the ducts with milk [5] Worldwide, breast cancer comprises 22.9% of all cancers (excluding non-melanoma skin cancers) in women .In 2008, breast cancer caused 458,503 deaths worldwide (13.7% of cancer deaths in women) [6] Breast cancer is more than 100 times more common in women than breast cancer in men [5].

For the breast cancer screening using microwaves, difference in the dielectric properties of healthy and cancerous breast tissues serves as the basis for this imaging technique. This was first reported in 1926 by Fricke and Morse and similar findings were confirmed later on. The difference in the permittivity between the two tissues is mainly due to the difference in their water content. The recent results by Chaudary [7] showed that the contrast at 1Ghz is about 4:1 in permittivity and 6:1 in conductivity.

Dielectric Properties

A dielectric material is an insulator which can be polarized when subjected to an Electric field. Every material has some electrical characteristics that are dependent on its permittivity and conductivity. These characteristics play a vital role in experimentation and accurate measurement is valuable information. To understand microwave tomography, it is required to get a detailed insight about these dielectric properties. Permittivity is a measure of how an electric field affects a dielectric and how much the material is polarized in response to that field. It is the materials ability to transmit electric field. Generally permittivity is not a constant and changes with temperature, frequency, mixture, orientation etc. Permittivity as a function of frequency can be real and can also take complex values. Consider a dielectric material as a lattice of neutral atoms. In an atom the positively charged nucleus is surrounded by a cloud of electrons and the overall charge is zero. In a dielectric material atoms have a good grip on their electrons and electrons cannot escape, whereas in a perfect electric conductor the atoms grip on their electron is approximately zero and hence current flows without resistance.

In presence of applied electric field positive nucleus is displaced slightly in one direction and electron cloud in the other, this displacement polarizes the atom, though the displacements are extremely small there is a significant total charge shift due to large number of atoms. This energy is stored as a form of mechanical energy in each atom. After the removal of the electric field the charges realign and the conserved energy is converted back to electric field.

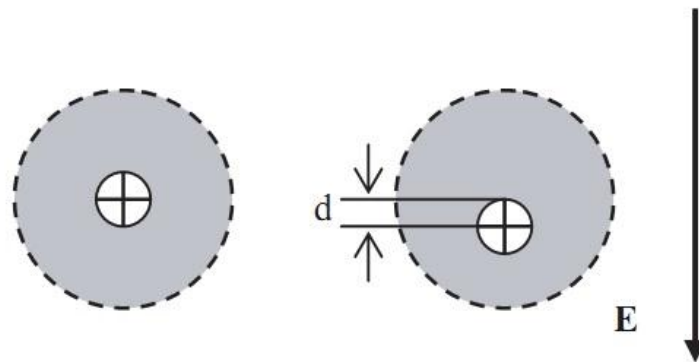


Figure 2-1: Nucleus Displacement in Atom

An opposed internal electric field is produced due to the charge displacement and its strength is related to the dielectric properties, this opposing field is called 'polarization field'. Permittivity of free space is

$$\epsilon_0 = 8.8541 * 10^{-12} \text{ F/m}$$

in SI units. The permittivity of all dielectrics is greater than that of vacuum. The common notation to describe permittivity of a dielectric material is 'relative permittivity'. The relative permittivity of some of the materials is given in the table below [11]:

Material	Relative Permittivity
Vacuum	1
Salt	3-15
Silicon	11.68
Methanol	30
Water (20 C)	80.1

2.1.1. Complex Permittivity

As mentioned earlier the response of material to electric field i.e. its permittivity depends upon the frequency of the applied field. The response is causal and can be represented by a phase difference. Hence to specify magnitude and phase, permittivity is often represented as a complex number. Complex permittivity in real and imaginary parts is denoted as:

$$\varepsilon(\omega) = \varepsilon'(\omega) + i \varepsilon''(\omega)$$

ε'' the imaginary part, describes the lossiness of the material

ε' the real part is the stored energy in the medium.

2.1.2. Conductivity

Flow of current is characterized by a parameter called conductivity represented by σ with SI units of Siemens per meter. When an external electric field is applied to the material, the electrons inside experiences the Coulombs force. Free charge carriers accelerated by this field collide with neighbouring electrons and thus charge is transferred. More the free electrons, more is the conductivity.

For perfect electric conductor (PEC) $\sigma = \infty$

For perfect electric insulator (PEI) $\sigma = 0$

To get a general idea conductivity values for some materials is in table below [12]:

Material	Conductivity
Iron	$1.0 * 10^7$
Sea Water	4.8
Drinking Water	$5.0 * 10^{-4}$

2.1.3. Biological Tissue Dielectric Properties

The object focused in our experimentation is Human Breast tissue, their dielectric properties are of interest as the final image is obtained with the reconstructed permittivity and conductivity.

Dispersive response

The human tissues have a dispersive response when exposed to electromagnetic radiations. Here dispersive response means that the conductivity and permittivity are dependent on the frequency of the incident electromagnetic waves. The cause of this dispersion is cell-membrane at lower frequencies and water molecules at higher frequencies, as explained by Cole [9].

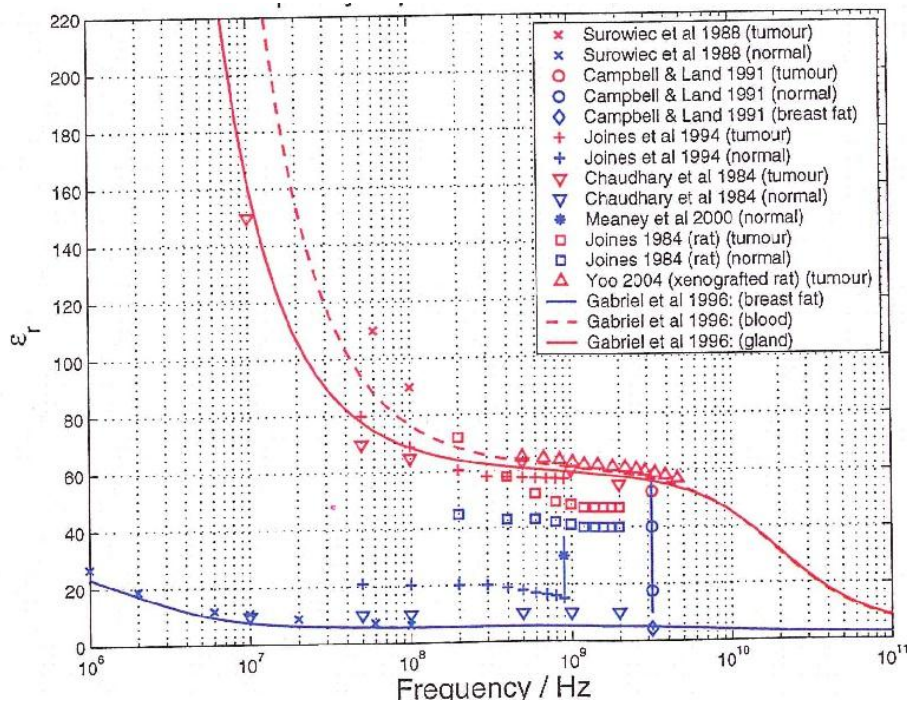


Figure 2-2: Frequency dependence of Permittivity, Literature values by Andreas Fhager, [1].

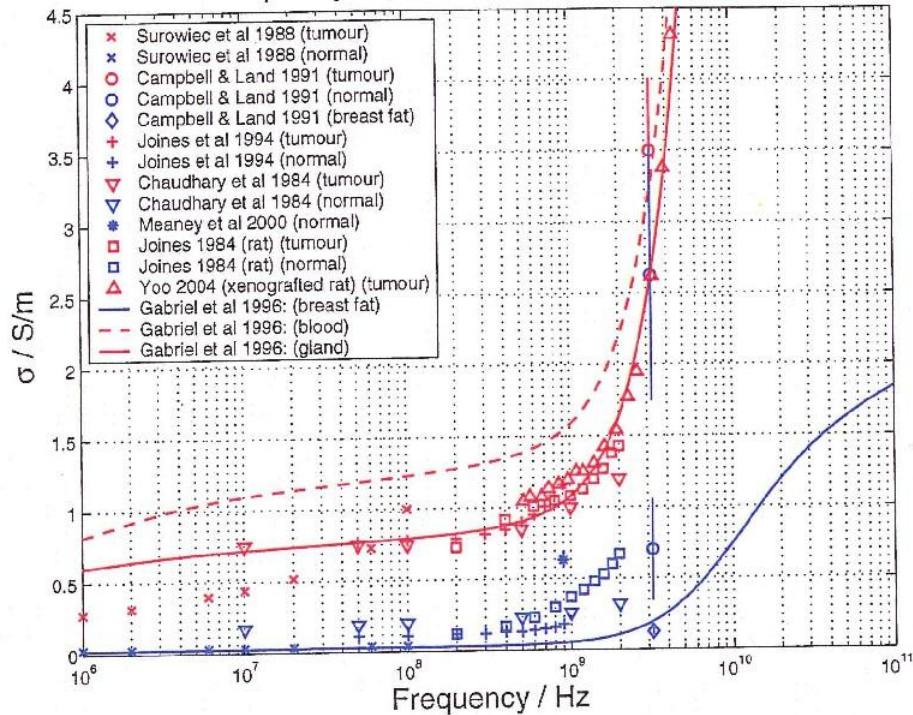


Figure 2-3: Frequency dependence of Conductivity, Literature values by Andreas Fager, [1].

The frequency span can be divided into three regions α , β and γ dispersion.

2.1.4. α Dispersion

At smaller frequencies, < 1 MHz there is high permittivity in body tissue. Proteins which build the cell membrane are large in size and exhibit a large dipole moment. Thus they induce a surface charge density and attract ions creating electric bi-layer. The relaxation of this electric bi-layer is one of the reasons of dispersive behaviour. Further details are not discussed as it would lead to a different topic. This dispersion is hardly noticeable in conductivity.

In short, the permittivity is highly effected by the cellular structure in this frequency range.

2.1.5. β Dispersion

At frequencies ranging between 10kHz and 10MHz β dispersion occurs and is due to the capacitive charging in the cellular membrane. Large dipole moments are possessed by hydrated proteins and dipolar relaxation of these molecules contribute to the dispersion in this frequency range.

2.1.6. γ Dispersion

At higher frequencies greater than 100 MHz the water content of the tissue, more of water molecules and presence of ions are largely determining the dielectric properties [1].

Di-Electric Model and Debye Equation

The aligning of the molecules and the ions to the applied electric field is not instantaneous. Different particles and different backgrounds will require different times for response.

Debye derived an equation for complex dielectric permittivity as a function of frequency, his derivations were made on a molecular.

The Debye equation is as follows:

$$\varepsilon^*(\omega) = \varepsilon_{inf} + \frac{\varepsilon_s - \varepsilon_{inf}}{1 + i\omega t}$$

A state conductivity is added to the equation above so as to incorporate existence of currents at infinite time, the new equation becomes

$$\varepsilon^*(\omega) = \varepsilon_{inf} + \frac{\varepsilon_s - \varepsilon_{inf}}{1 + i\omega t} - \frac{\sigma_s}{\omega t}$$

More complex dispersive behaviour can be represented by superposition of first order process. Cole and Cole [9] suggested an empirical formula for modelling dielectric properties of tissue given as:

$$\varepsilon^*(\omega) = \varepsilon_{inf} + \sum_n \frac{\Delta\varepsilon_n}{1 + (i\omega t)^{(1-\alpha_n)}} + \frac{\sigma_s}{\omega t}$$

The parameters are chosen appropriately for each tissue, by fitting data from measurements to this equation [1].

2.1.7. Maxwell equations

Maxwell's equations form the foundation of classical electromagnetic phenomena. They describe how electric charge and electric currents act as a source for electric and magnetic field. Moreover the generation of time varying magnetic field from time varying electric field and vice versa is also explained. These equations in differential form are stated as follows:

$$\begin{aligned}\nabla \cdot \mathbf{D} &= \rho \\ \nabla \cdot \mathbf{B} &= 0 \\ \nabla \times \mathbf{E} &= -\mathbf{J}_m - \frac{\partial \mathbf{B}}{\partial t} \\ \nabla \times \mathbf{H} &= \mathbf{J}_e + \frac{\partial \mathbf{D}}{\partial t}\end{aligned}$$

The influence of different on electromagnetic waves is explained by their dielectric properties these properties are described by the following equations:

$$\begin{aligned}D &= \epsilon E \\B &= \mu H \\J_e &= \sigma E \\J_m &= \sigma' H\end{aligned}$$

Where ϵ is the permittivity,
 μ is the permeability,
 σ is the conductivity and
 σ' is the magnetic loss.

3. The Experimental Setup

As mentioned earlier, the transmission and reflection data is required for the construction of the image. These measurements are performed with the Agilent E8362B network analyzer. The ports on this device are used to transmit and receive data. The four scattering parameters for a two port network can be explained by the following figure.

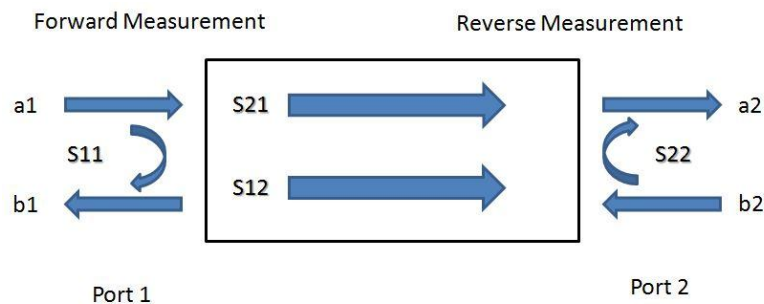


Figure 3-1: Scattering parameters for a Two-Port network

The relation between the s-parameters and the incident and reflected wave is given by the following matrix:

$$\begin{pmatrix} b_1 \\ b_2 \end{pmatrix} = \begin{pmatrix} S_{11} & S_{12} \\ S_{21} & S_{22} \end{pmatrix} \begin{pmatrix} a_1 \\ a_2 \end{pmatrix}$$

Given the impedance is matched at the load, b₂ will be totally transmitted making a₂ = 0. Therefore:

$$S_{11} = \frac{b_1}{a_1} \quad \& \quad S_{21} = \frac{b_2}{a_1}$$

Similarly if the input port is matched then a₁ = 0 and

$$S_{12} = \frac{b_1}{a_2} \quad \& \quad S_{22} = \frac{b_2}{a_2}$$

Where

S₁₁ = Input port voltage reflection coefficient

S₁₂ = Reverse transmission coefficient

S₂₁ = Forward transmission coefficient i.e. the Gain

S₂₂ = Output voltage reflection coefficient

Physical Parameters Summary

Height of the water tank:	275 mm
Diameter of water tank:	400 mm
Length of Antenna cable:	1.5 m
Length of Antenna Conductor:	150 mm
Number of Antenna Bent:	20 mm
Liquid inside tank:	Salt water

To get a general idea of physical dimensions of experimental apparatus, a few images were taken and a summary is presented in tabular form.

The cylindrical tank has twenty four openings to fit in antennas in a circular pattern. Diameter of this tank is 400 mm and is 275 mm deep. The length of Antenna's outer conductor is around 150 mm as seen in the Figure 3.2.

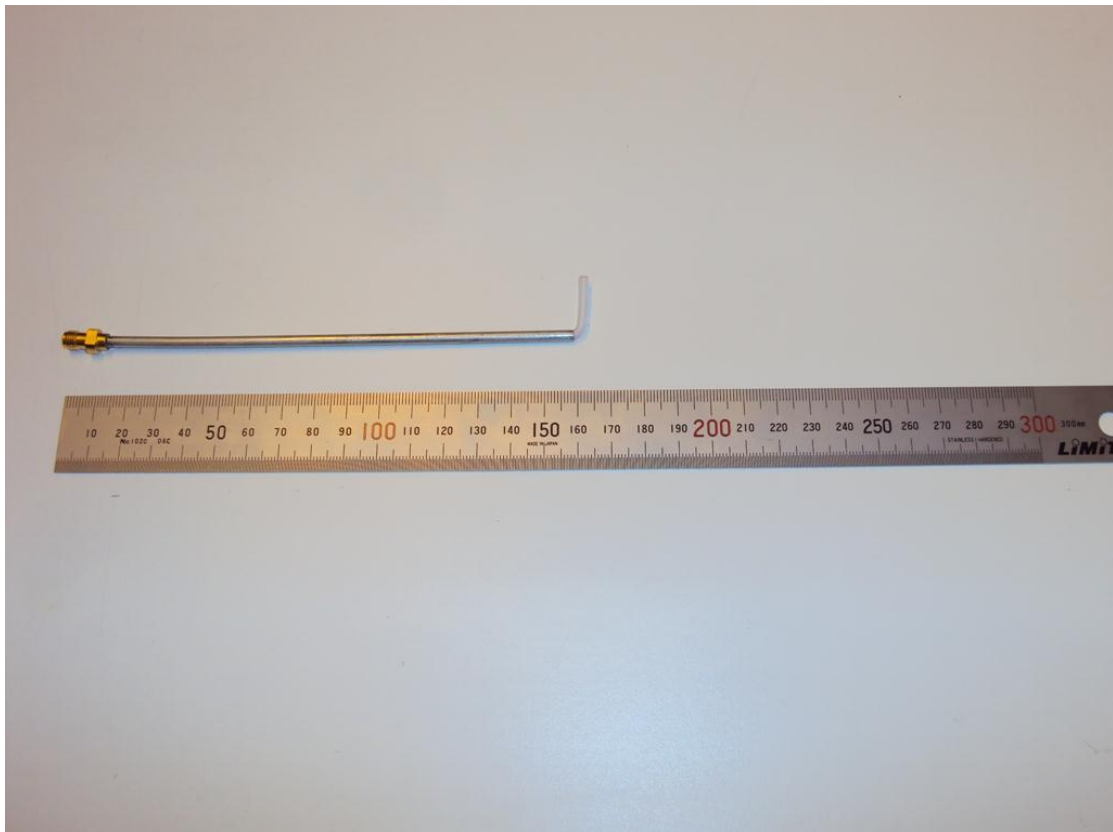


Figure 3-2: Antenna Length Measurement

Figure 3.3 shows the dimensions of the imaged objects. The cup used for imaging is comparable to physical dimensions of female human Breasts. A screw positioned within the cup is comparable to tumour within the breasts.



Figure 3-3: Length Comparison, Cup, Acrylic Cylinder and Metal Screw

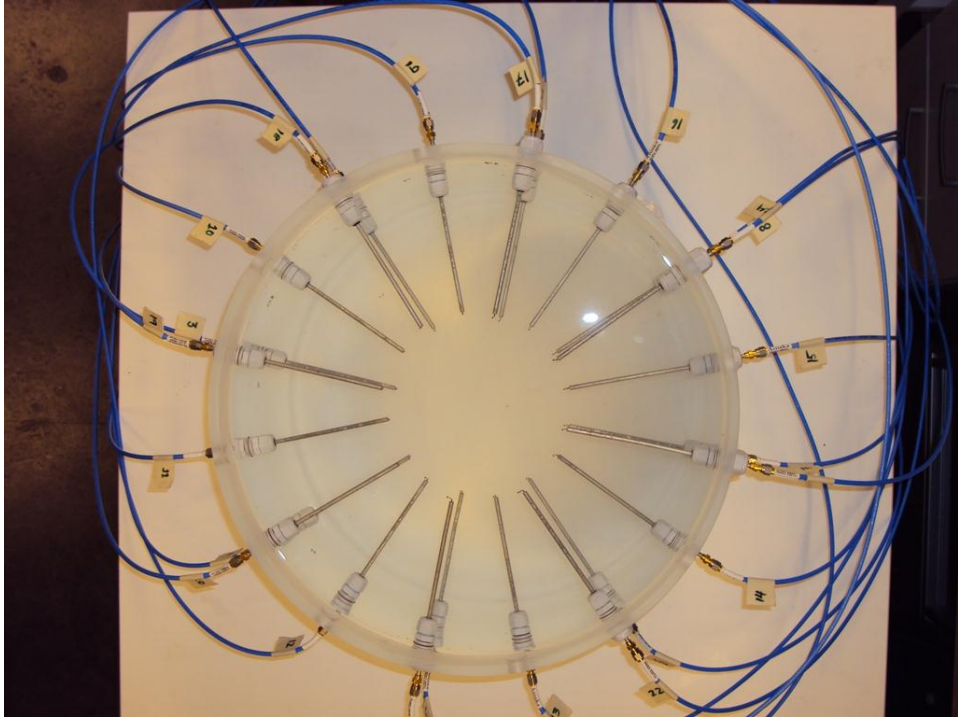


Figure 3-4: Top view, Measurement tank filled with water

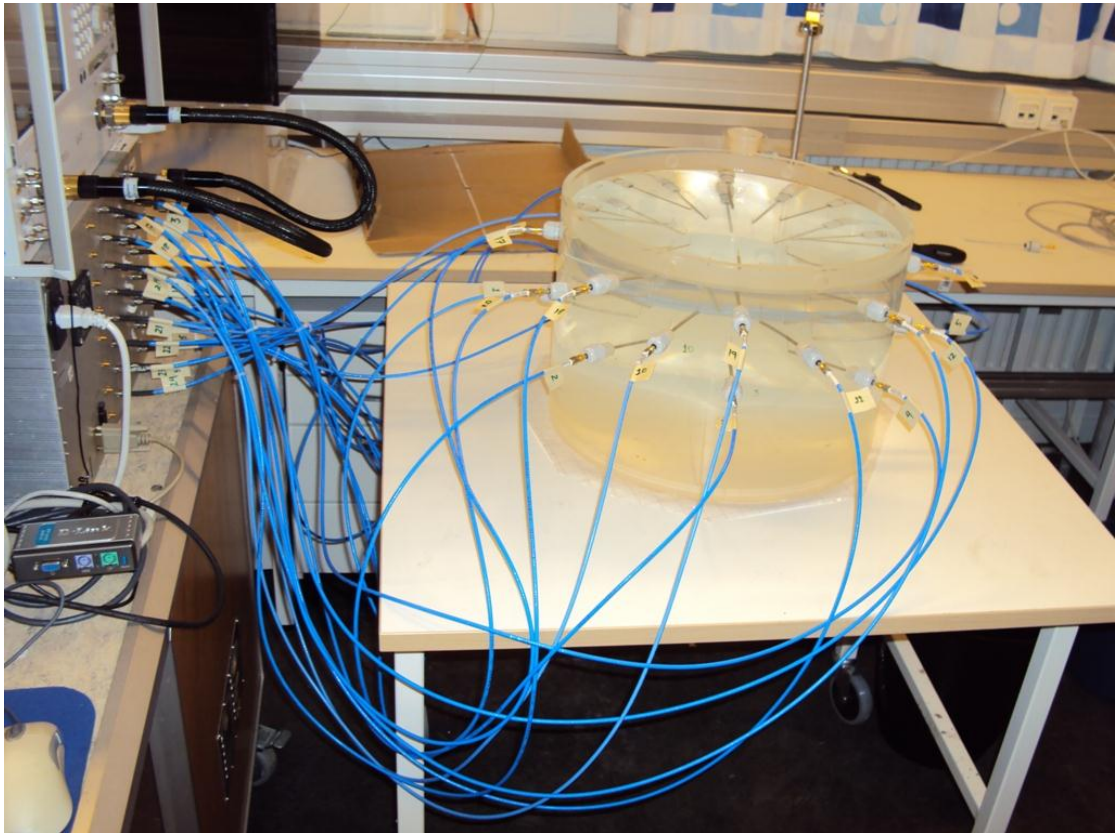


Figure 3-5: Side View, Measurement System connected to a PNA

Figure 3.4 and Figure 3.5 are images of a working prototype. The blue cables are connected to a switching matrix, which switches the antenna and give corresponding signal to the network analyser. The cables are labelled and so is the Switch to avoid any error and mixing of data. The final equipment would be a treatment couch, equipped with circular openings for the breasts, so that patient can be examined with relative ease.

Simulated Parameters Summary

Size of Domain/ Grid Size:	98 * 98 * 74
Spatial Step Length:	4.0 mm * 4.0 mm * 4.0 mm
Simulation Time:	20 e-9 sec
Type of source function:	EXP-COS-SINC
Centre frequency of the Source:	700 MHz
Bandwidth of the source:	500 MHz
Number of antennas:	24

Up gradation of Existing Prototype

Existing setup was a cylindrical tank with twenty four antennas in three layers in a circular pattern. The antennas were not firmly attached to the cylindrical walls; a small movement altered the position of the antenna. For best results, accuracy of antenna positions was necessary. Additional holders were internally threaded and were attached to each antenna, thus providing rigidity. All antenna cables were labelled and tied to avoid human error.

4. The FDTD Modelling

Image Reconstruction

The image of the dielectric properties is reconstructed from the measurement data obtained from the antenna array placed in the middle of the tank. For the construction of an image, iterative time-domain inversion algorithm is used developed by Fhager [1], which reconstructs the dielectric properties of the object, FDTD simulations of *Electromagnetic problem* with the computations of a *Adjoint-Maxwell problem* are used to compute gradient. This gradient is then optimised in a *conjugate gradient optimisation algorithm* [1].

Scattering data from a transient pulse is taken, this measurement data obtained from the antenna array system i.e. the network analyser, is in frequency domain, which is converted into time domain with Inverse Fourier Transform. This data is compared with the numerical simulation of the system. Initially all of the grid cells are assigned uniform background properties which are then updated. The difference between the measured and simulated electric fields updates the dielectric properties of the target under construction. With each iteration the target object is refined and the simulated and measured signals converge. When the difference between the simulation and measurement is small enough, the minimisation stops and the dielectric properties are updated.

Calibration of the system is performed to incorporate effect of the cables and the medium. This calibration is done with help Electronic Calibration Module by Agilent systems specifying the frequency band, number of sample points and type of frequency sweep method. Besides electronic calibration, another calibration is performed by measuring an empty system. The resulting calibrated E-field is obtained as follows:

$$E_{cal} = \frac{S_{obj}}{S_{ref}} * E_{sim}$$

Where

S_{obj} is the measured scattering parameter with object present

S_{ref} is the measured scattering parameter with an empty system

E_{sim} is the simulated electric field.

The aim of the reconstruction procedure is the minimisation of the functional defined as:

$$F(x) = \int_0^T \sum_{m=1}^M \sum_{n=1}^N (|E_m - E_m^{meas}|^2) dt$$

where E_m is the calculated field from the computational model and E_{meas} is the measured data. M and N are the number of transmitters and receivers respectively. The minimisation was achieved with a conjugate gradient algorithm, as mentioned earlier. This algorithm and its modification was not in the scope of my work for further details one can refer to Polak [12] and Fhager [1].

FDTD Modelling

Finite-difference time-domain (FDTD) is computational electrodynamics modelling technique used to solve Maxwell's equations. It is a time domain method so the solution can cover wide range of frequencies. It employs finite differences as approximation to the derivatives in Maxwell equations. The resulting finite difference equations are solved in a leap-frog manner [7]. The electric field components are solved at a given instant of time and then the magnetic field components are solved at the next instant of time, the process is repeated until a steady state EM behaviour is computed. The vector components of Maxwell equations give the following equations:

$$\begin{aligned}\frac{\partial H_x}{\partial t} &= \frac{1}{\mu} \left(\frac{\partial E_y}{\partial z} - \frac{\partial E_z}{\partial y} - \sigma' H_x \right) \\ \frac{\partial H_y}{\partial t} &= \frac{1}{\mu} \left(\frac{\partial E_z}{\partial x} - \frac{\partial E_x}{\partial z} - \sigma' H_y \right) \\ \frac{\partial H_z}{\partial t} &= \frac{1}{\mu} \left(\frac{\partial E_x}{\partial y} - \frac{\partial E_y}{\partial x} - \sigma' H_z \right) \\ \frac{\partial E_x}{\partial t} &= \frac{1}{\varepsilon} \left(\frac{\partial H_z}{\partial y} - \frac{\partial H_y}{\partial z} - \sigma E_x \right) \\ \frac{\partial E_y}{\partial t} &= \frac{1}{\varepsilon} \left(\frac{\partial H_x}{\partial z} - \frac{\partial H_z}{\partial x} - \sigma E_y \right) \\ \frac{\partial E_z}{\partial t} &= \frac{1}{\varepsilon} \left(\frac{\partial H_y}{\partial x} - \frac{\partial H_x}{\partial y} - \sigma E_z \right)\end{aligned}$$

The basic time stepping relation as explained by Yee [8], at any point in space the updated value of Electric field is dependent on the stored value of the Electric field and the curl of Magnetic field. The magnetic field is time stepped similarly.

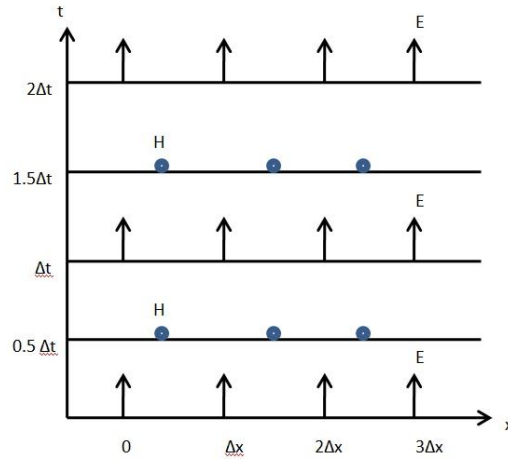


Figure 4-1: Time Stepping Electric and Magnetic field

Iterating the E-Field and H-field results in the marching in time process where sampled data of continuous EM waves propagate in the numerical grid stored in the computer memory [7].

Different field components are stored for different grid locations, the resulting structure as shown below is known as the Yee Lattice.

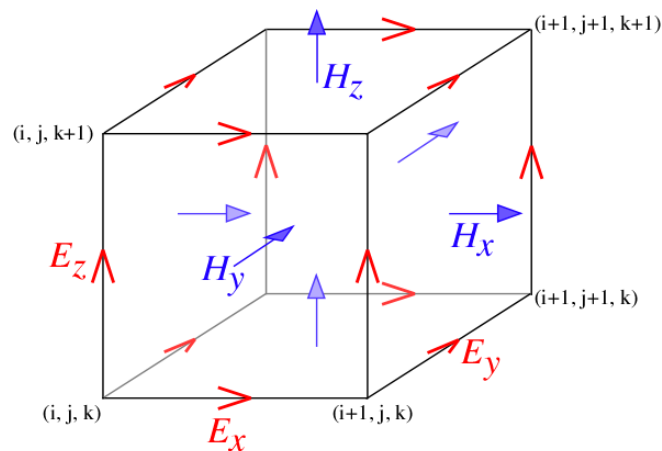


Figure 4-2: The Yee Lattice

Antenna Modelling

In our experiment setup many different types of antennas could have been used, but monopole antennas were selected as they can be modelled with ease. A simple monopole consists of a straight rod shaped conductor; in fact any metal wire/cable can act as a monopole antenna when attached to a transmitter. Monopole antenna is a dipole antenna with one pole substituted as a ground plane. In the modelling of

antennas there is no ground plane so the antennas are modelled in a slight different way. Ground plane is modeled as PEC with E-field components set to zero. Thin-wire approximation is used to model the antenna wire.

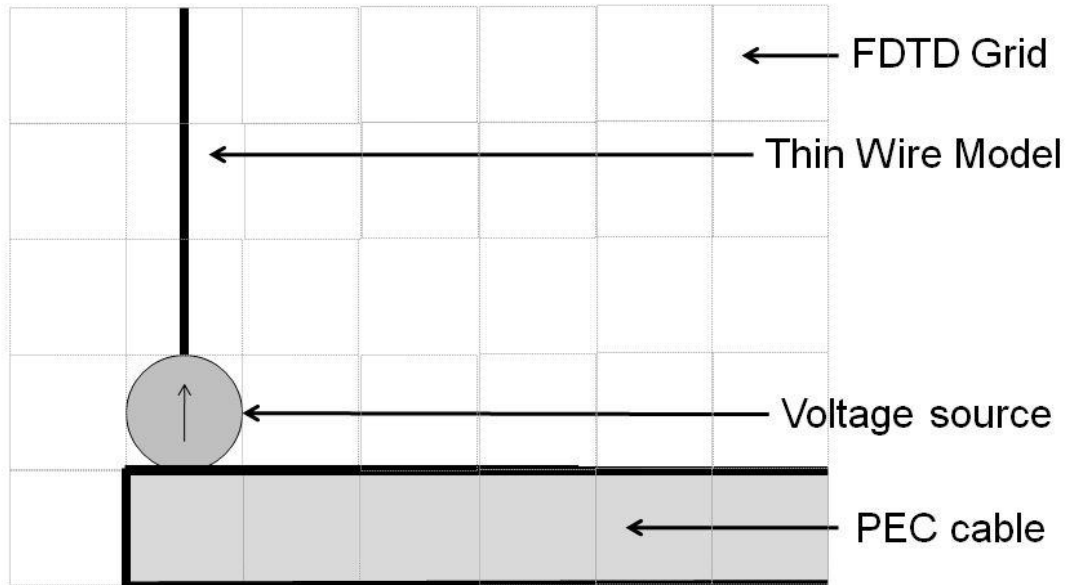


Figure 4-3: FDTD Modelled Antenna

The active antennas are modelled as a thin wire, i.e. a fraction of the grid cell, consisting of a Perfect Electric Conductor (PEC) which corresponds to an E -field with all tangential components set to zero. In reality the metal wire is a PEC which is modelled as setting the E -field components that corresponds to the metal surface to zero. This will give the boundary condition that no electric field is present on the metal wire's surface. The wire carries a current and thus the surrounding H -components are affected. All the H -components vary by $1/r$ where r is the distance to the wire and the axial E -components that are aligned with the antenna are set to zero [13,14].

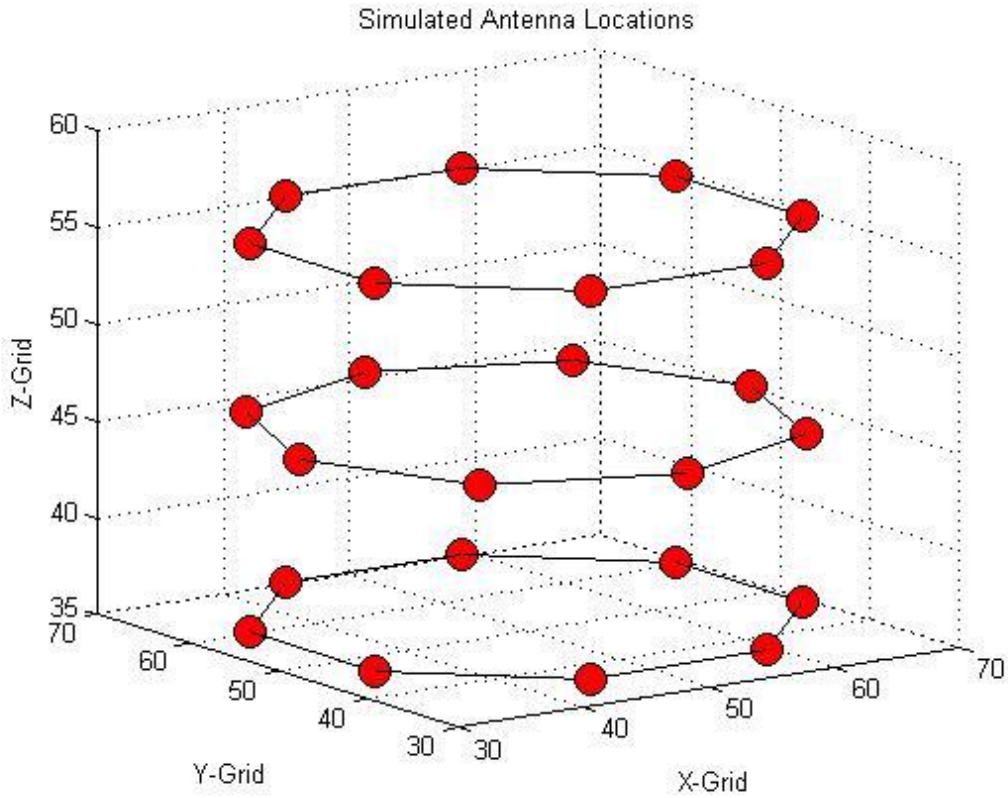


Figure 4-4: Antenna locations in a 3D-Grid used in Simulation

Figure 4.4 shows the locations of the transmitters/receivers in three circles within the 3-dimensional grid. This figure represents the simulated antenna locations and can be compared with figure 3.5 which shows the actual experimental setup.

Measured Antenna Data vs. Simulated Data

The appropriate length of antenna was a crucial part as the operating microwave frequency has a direct relation to the length of the antenna. Moreover, there is a specific part of the spectrum where there was a high contrast in the dielectric properties of tumour. This specific frequency range was from 300 MHz up to 3 GHz. The length of the quarter wave monopole is given as

$$l = \lambda/4$$

Where,

$$\lambda = v_p / f$$

And,

$$v_p = c / \sqrt{\epsilon_r}$$

Different lengths were calculated and measured but the best results with the required frequency were with 20 mm antenna length. The S11 plots for various antenna sizes can be seen in the figure below.

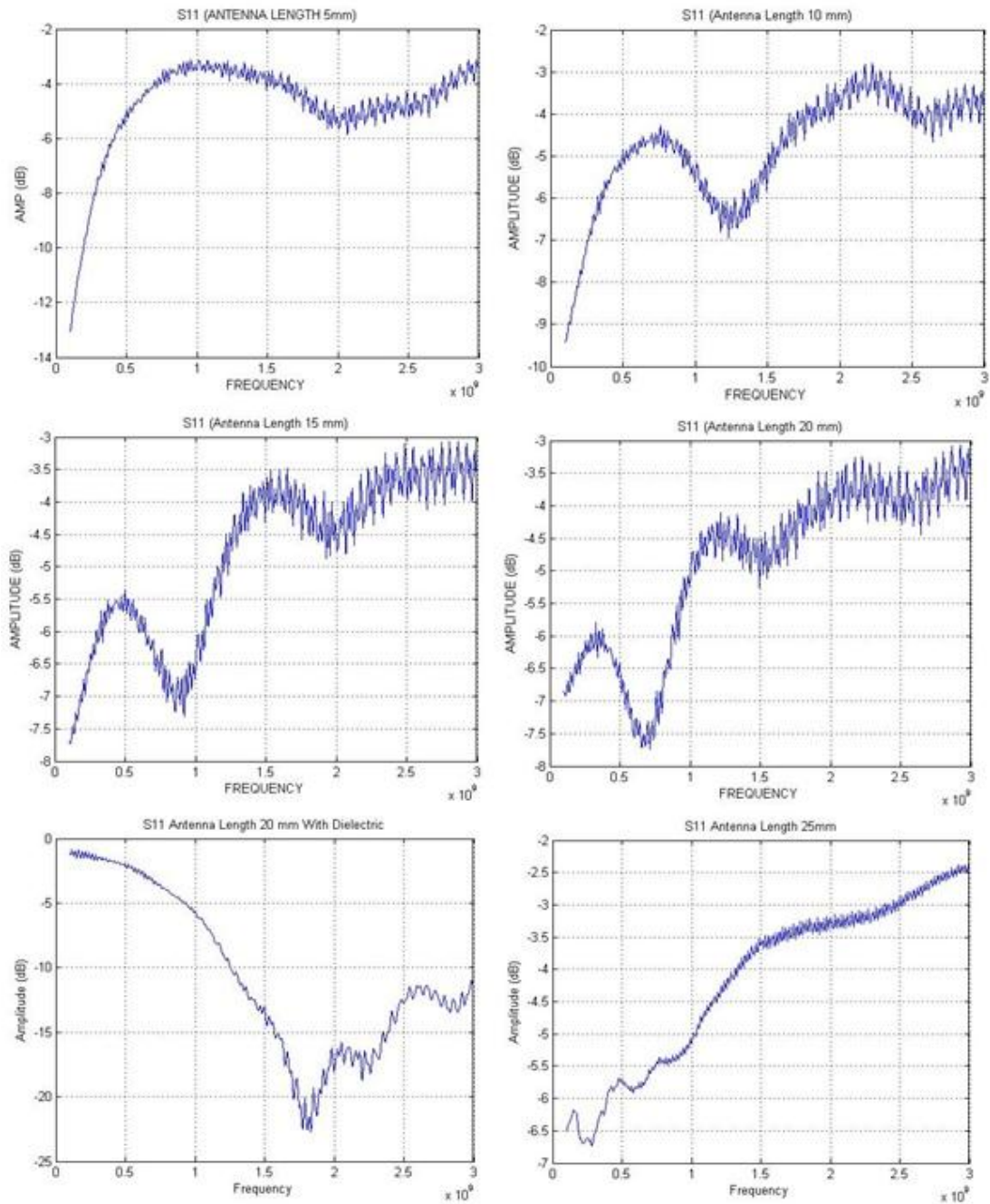


Figure 4-5: S11 parameter plot at different Antenna Lengths

The S11 as mentioned earlier is the voltage reflection coefficient; this parameter defines the efficiency of an antenna. The S11 curves have a minimum at a frequency which is called the resonance frequency; this is where the antenna has the lowest

amount of reflection at said frequency. Monopole antennas with amplitude below -10 dB at the resonance frequency are considered good. In figure 4.5 we see that the antennas do not have a sharp resonance frequency. Little distortion can be seen in the plots as each antenna was not calibrated separately. A gradual change in the plots can be seen as the length was varied. With 20mm antenna length the amplitude of reflection coefficient was minimum. When the length was increased up to 25mm the minima shifted which was outside of frequency under observation.

Water Tank Modelling

A lossy medium was required to be modelled within the domain so that the currents in the outer conductor are attenuated, which would have been very difficult to model otherwise.

Water was used as a lossy medium; table salt was added to increase conductivity. The background relative permittivity was 78 and background conductivity was set to 0.2.

Multi-Grid Approach

In the FDTD Modelling size of the grid was a critical factor, as its size determined the computational cost for the image construction. We were limited by memory size on our servers. To obtain a better resolution of image and resolve smaller objects a greater grid size was required.

As it was seen that the antenna with the dielectric on had a better performance, this dielectric was small so as to be resolved with the existing grid size.

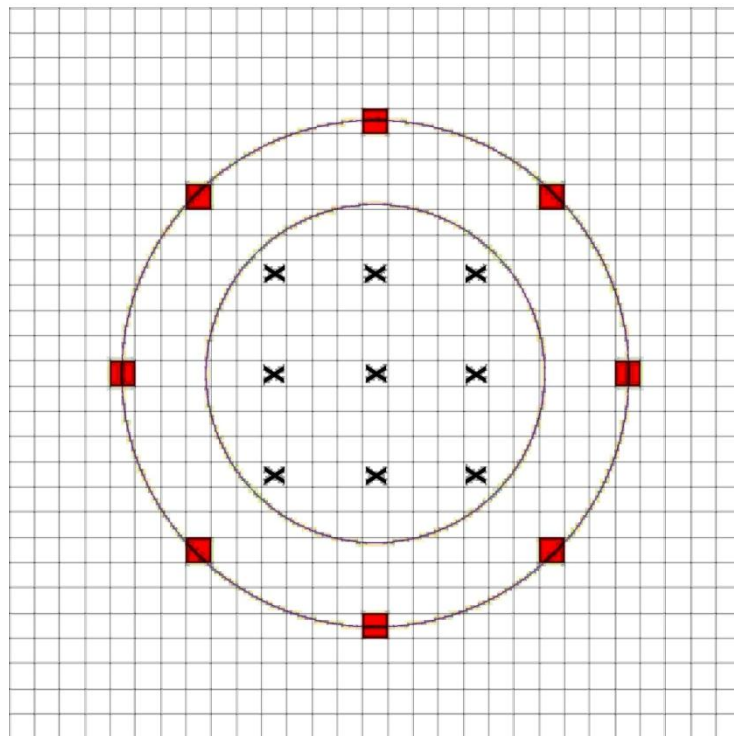


Figure 6-6: One mm Resolution Grid with Antennas

With multi Grid approach we are able to perform reconstruction on multiple grid sizes instead of a uniform grid. For instance a multi grid, 4:1 would have worked as follows: A complete 1mm grid should be calculated and updated, whereas with in the reconstruction domain gradient values for every fourth grid cell are computed and updated. For the neighbouring cells the values can either be extended or interpolated by any method of interpolation. By this method the resolution of modelled dielectric coated antennas to a finer grid of 1mm resolution was possible whereas overcoming all sorts of memory errors and limitations. Figure 4.6 shows a 1mm resolution grid, with the red cells representing transmitters and receivers locations in a two dimensional view. The marked cells show the calculated gradient values in every fourth cell with in the reconstruction domain.

5. Results and Discussion

Measured Permittivity

The permittivity of various liquids used was measured using a dielectric probe for a given range of frequencies.

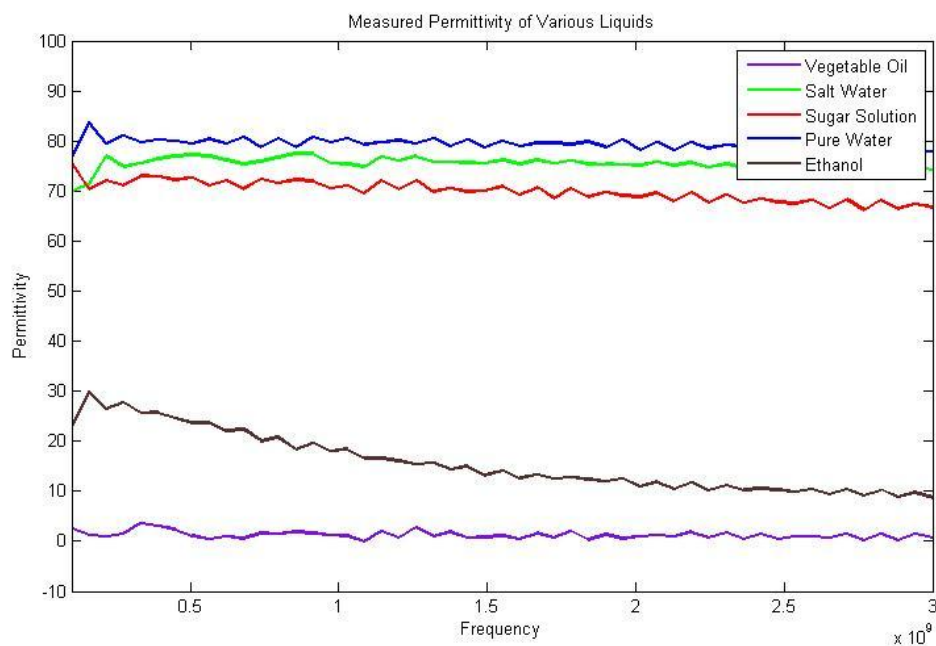


Figure 5-1: Measured Permittivity

Salt water was used as a matching liquid so as to reduce the dielectric contrast between medium and object being imaged. There was a significant contrast in the permittivity when the object was vegetable oil and background was salt water. This contrast is visible in the measurement. The reconstruction algorithm was successfully able to converge the functional. Reconstruction was also successful when contrast was slightly reduced and ethanol was used as an object. Finally reconstruction was unsuccessful when sugar solution was used as an object and the algorithm was unable to converge. This is discussed latter in the chapter.

One Acrylic Cylinder

5.1.1. Permittivity

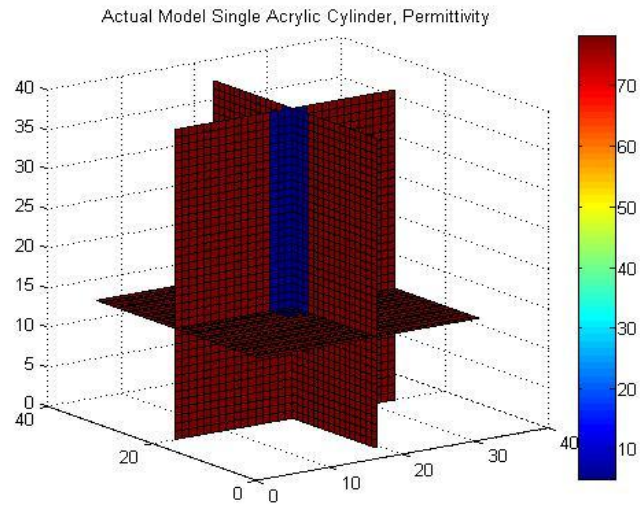


Figure 5-2: Actual Model Single Acrylic Cylinder, Permittivity

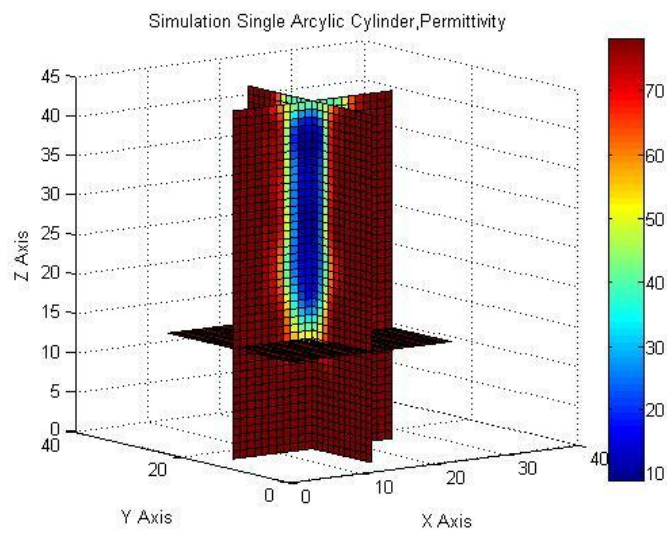


Figure 2

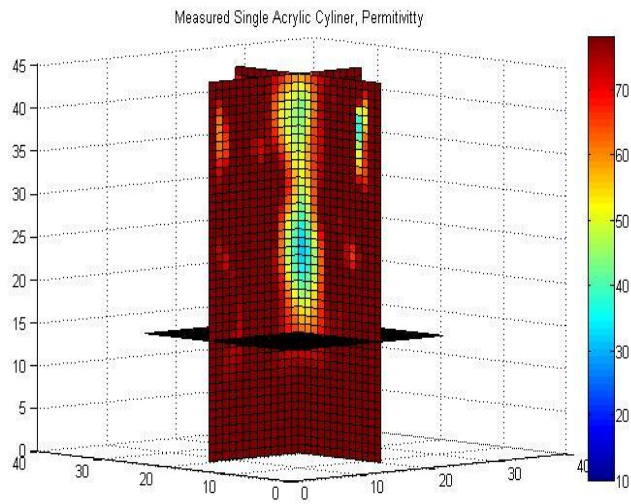


Figure 5-4: Measured Single Acrylic Cylinder, Permittivity

5.1.2. Conductivity

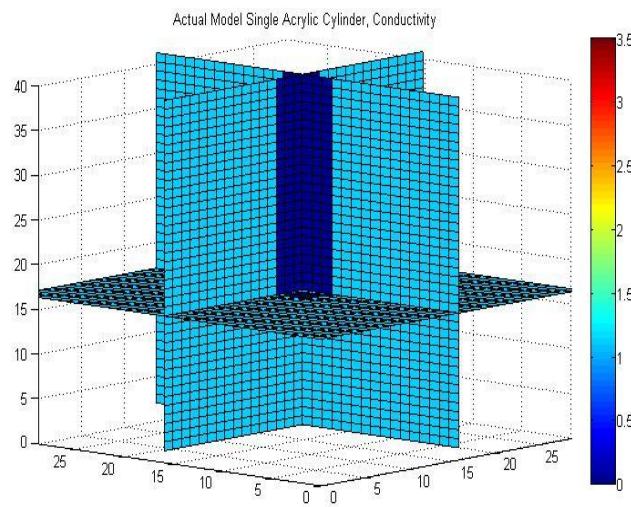


Figure 5-5: Actual Model Single Acrylic Cylinder, Conductivity

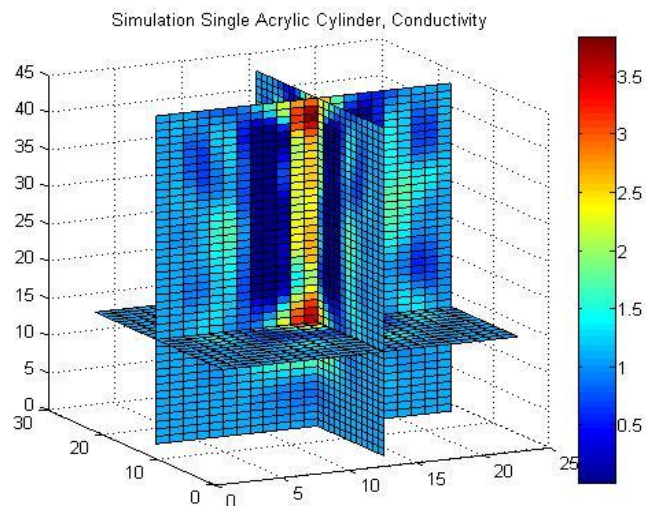


Figure 5-6: Simulation Single Acrylic Cylinder, Conductivity

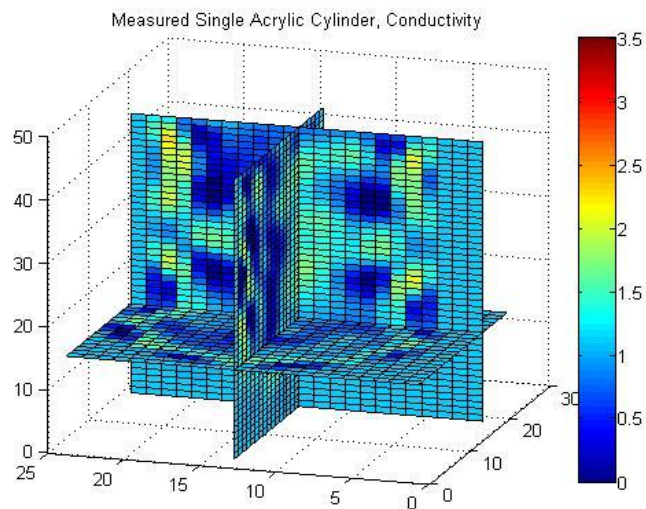


Figure 5-7: Measured Single Acrylic Cylinder, Conductivity

The object imaged in the figure above is an Acrylic cylinder of length 170 mm and a diameter of 15 mm. The cylinder was placed in the middle of the water tank and was immersed in salt water. The first image is the modelled acrylic cylinder within the tank and was modelled as a dielectric cylinder with the Permittivity set to 3. All the images are sliced in the x-plane and y-plane at the centre of the object to get a complete insight of the object's dielectric values. The reconstructed measurement data shows good similarity to the reconstruction of simulated data for the permittivity; however there are a lot of artefacts in the reconstruction of measured data for the conductivity. The permittivity reconstructed in the simulated data was 10, whereas permittivity of measured data was 30. The actual permittivity of the acrylic material was 3 as it was set in the model.

Two Acrylic Cylinders

5.2.1. Permittivity

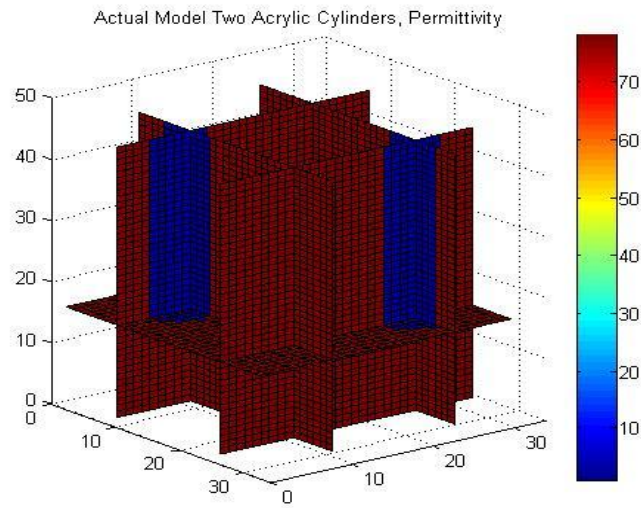


Figure 3

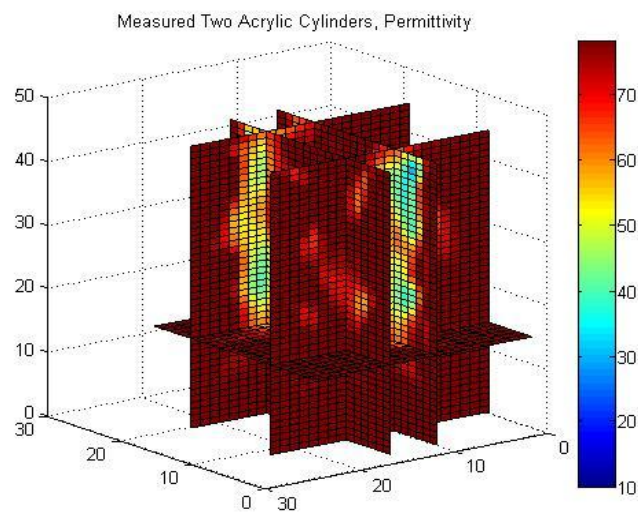


Figure 4

5.2.2. Conductivity

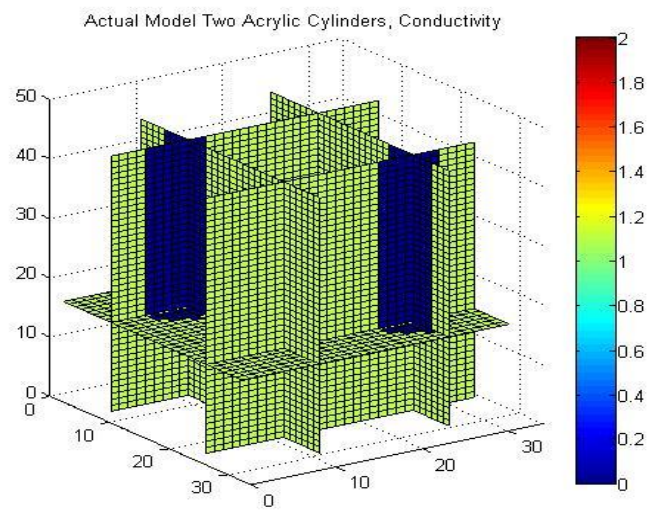


Figure 5

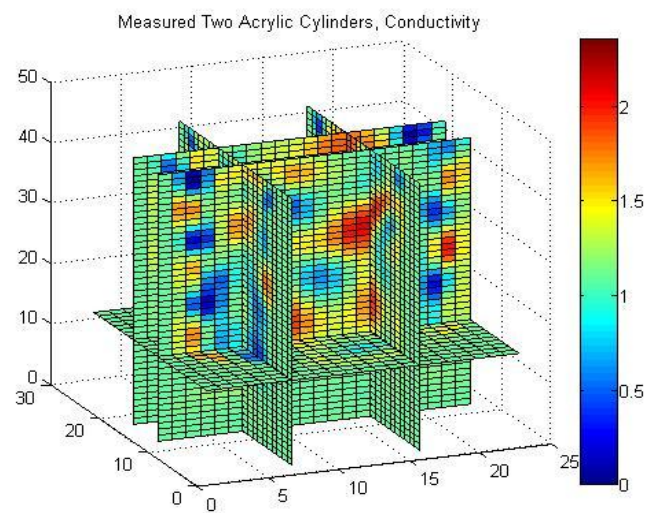


Figure 5-11: 6

Now instead of one, two acrylic cylinders of same length were imaged. The cylinders were placed at a fixed distance and it was modelled so. The results were similar to that of a single cylinder and was expected so.

Vegetable Oil Cylinder

5.3.1. Permittivity

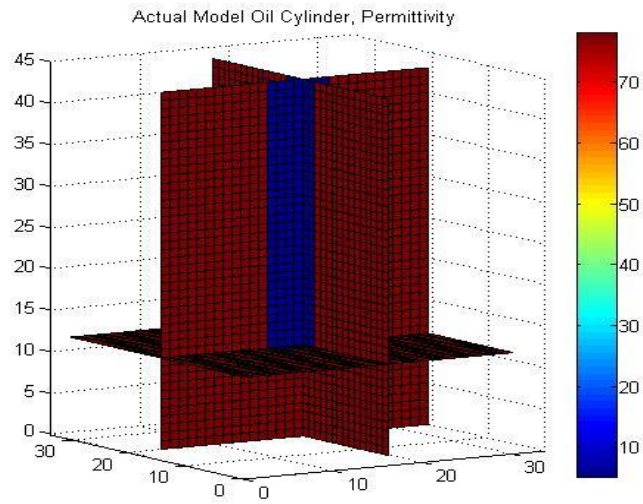


Figure 5-12: Actual Model Vegetable Oil Cylinder, Permittivity

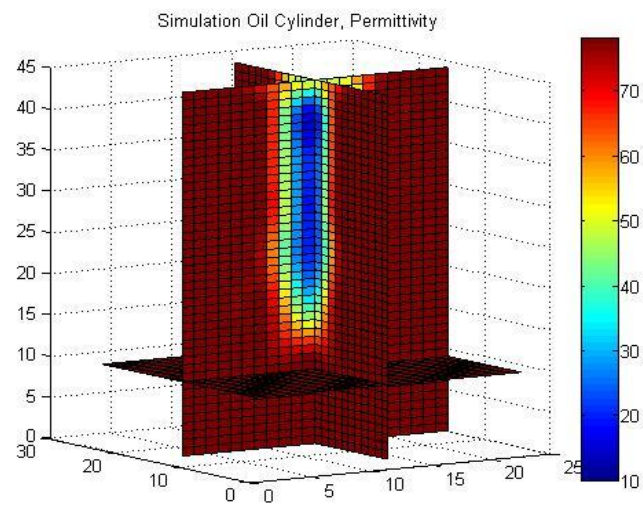


Figure 5-13: Simulation Vegetable Oil Cylinder, Permittivity

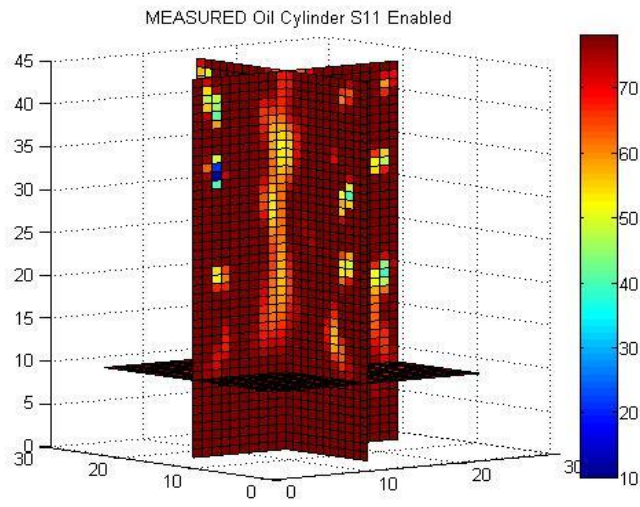


Figure 5-14: Measured Vegetable Oil Cylinder, Permittivity (S11 Enabled)

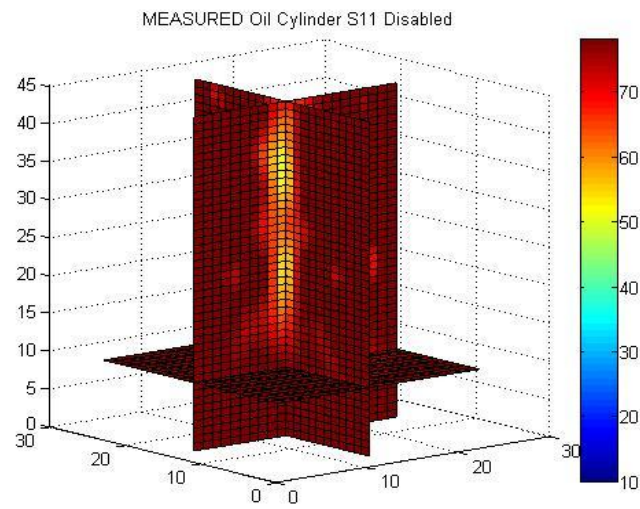


Figure 5-15: Measured Vegetable Oil Cylinder, Permittivity (S11 Disabled)

5.3.2. Conductivity

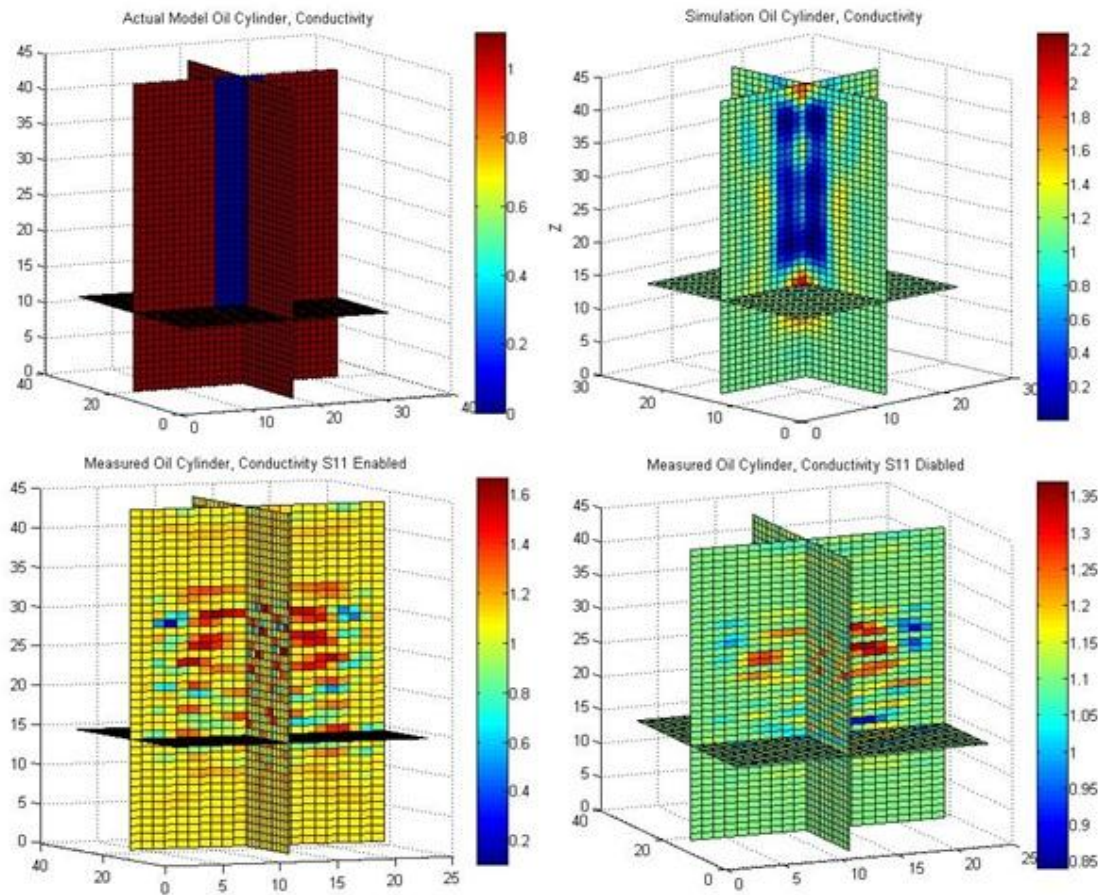


Figure 5-16: Vegetable Oil Cylinder, Conductivity

The next object imaged was a thin glass cylinder filled with oil. The permittivity of vegetable oil is around 4, and has somewhat similar properties to human fat tissue. A variation in the reconstruction was also observed by enabling and disabling the S11 parameter during the image reconstruction of the measured data. It can be seen that the simulation had a better agreement with the measured data when S11 was disabled. When the reflection (S11) and transmission (S12) scattering data were plotted, the amplitude of transmission coefficient was very small compared to that of the reflection coefficient. Thus when enabling the use of S11 parameter during the reconstruction the actual measured data was suppressed and noise became dominant hence artefacts can be seen in the reconstruction.

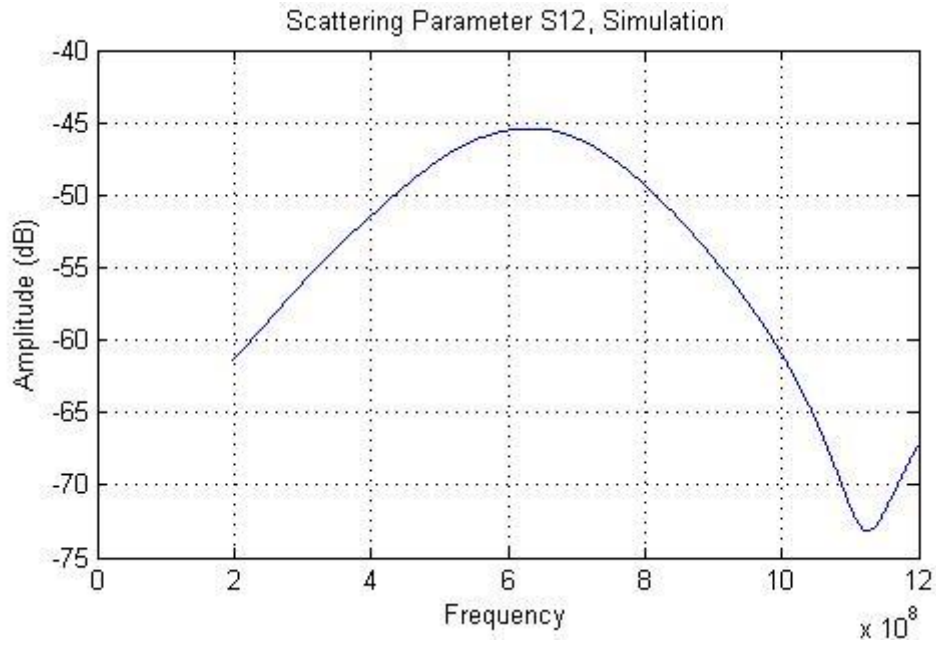


Figure 5-17: Simulated S12 Plot, Antenna 1-2

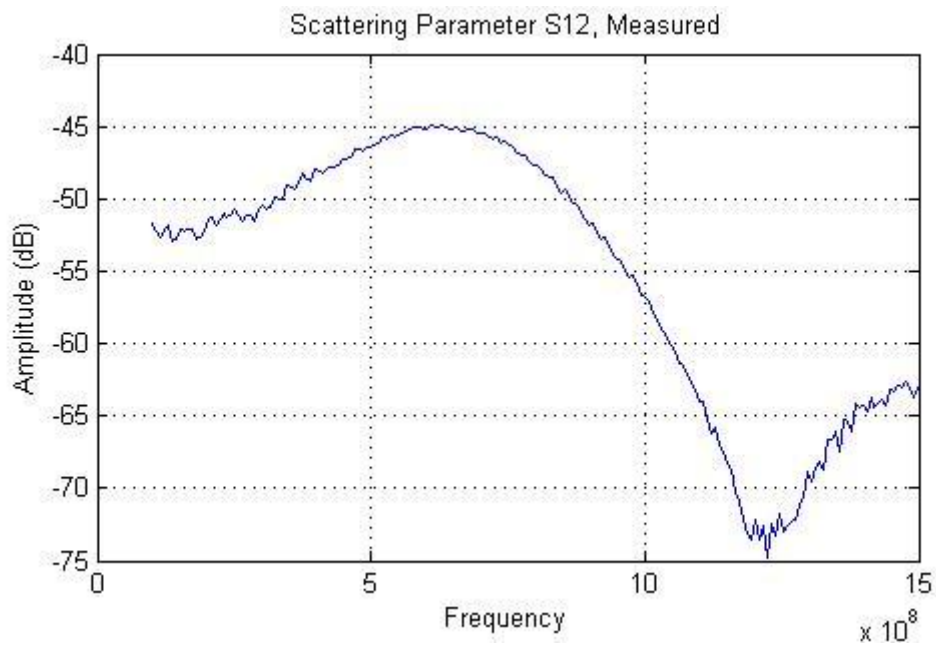


Figure 5-18: Measured S11 Plot, Antenna 1-2

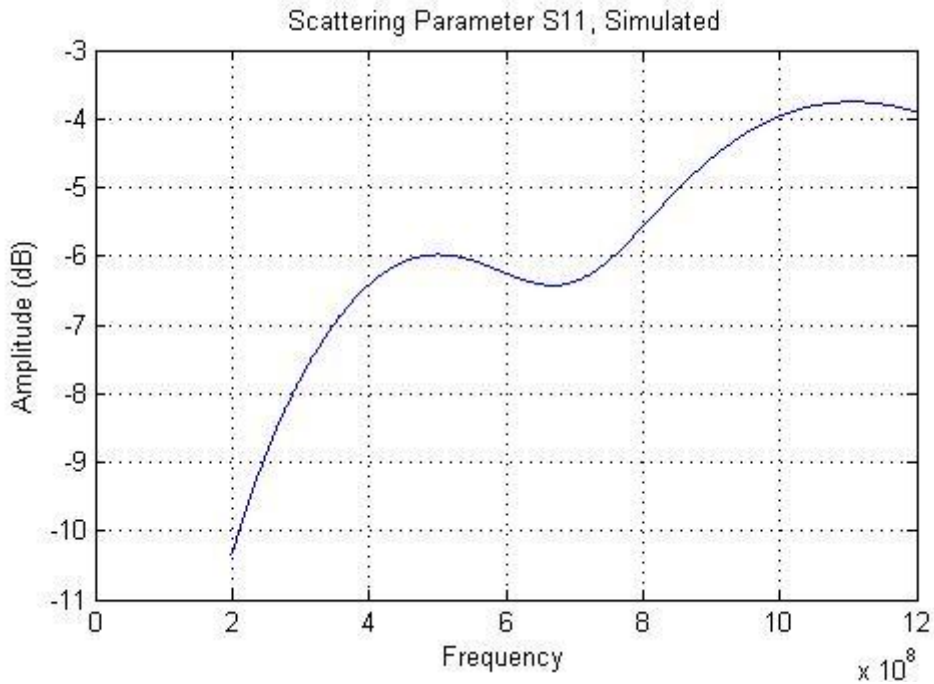


Figure 5-19: Simulated S11 Plot, Antenna 1

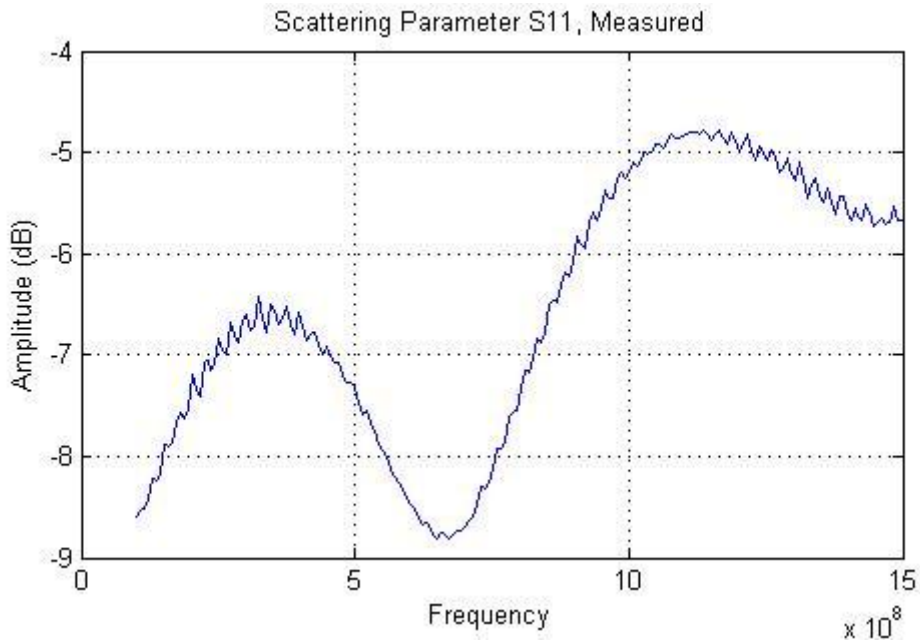


Figure 5-20: Measured S11 Plot, Antenna 1

The measured antenna scattering plots with their simulation counter parts are compared where the difference in the amplitudes is visible in the transmission (S12) and reflection (S11) coefficients. A slight error in the S11 data will result in a large error in the reconstruction as the amplitude is much higher compared to that of S12.

Ethanol Cylinder Multi Grid (2 mm)

5.4.1. Permittivity

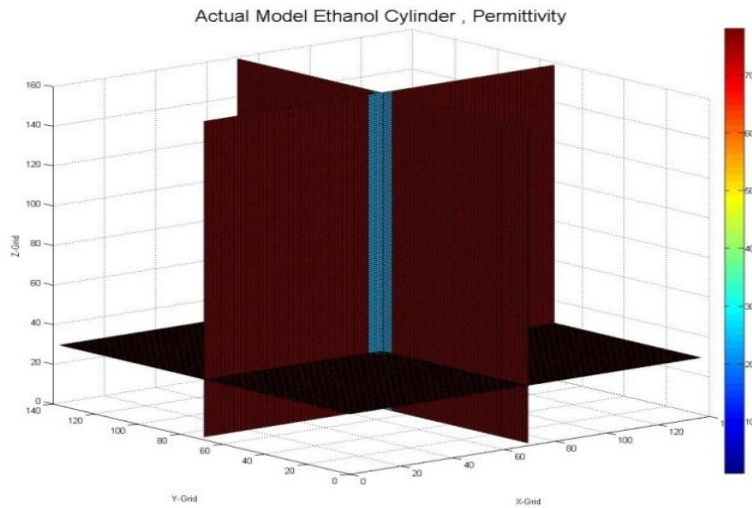


Figure 5-21: Modelled Ethanol Cylinder, Permittivity

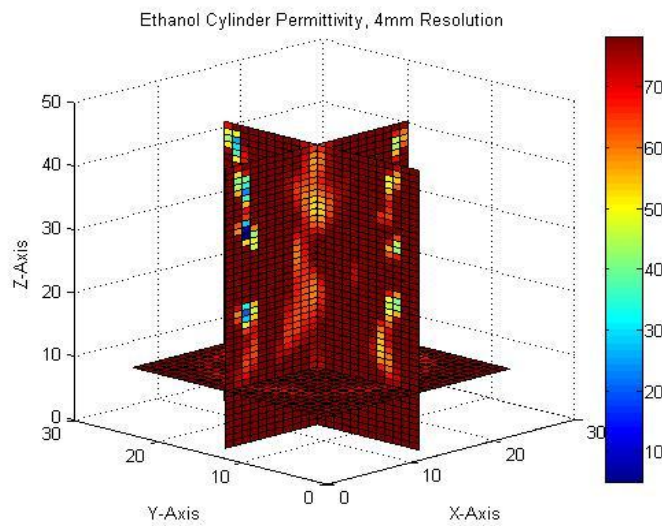


Figure 5-22: Measured Ethanol Cylinder, Permittivity (4mm)

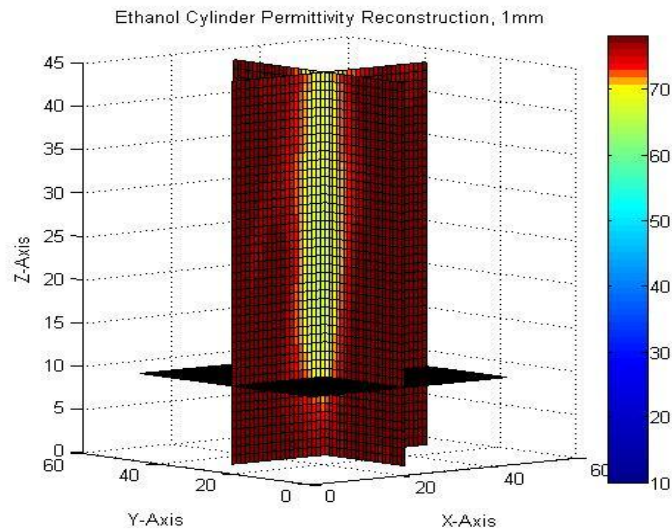


Figure 5-23: Measured Ethanol Cylinder, Permittivity (2mm)

This was a glass tube filled with ethanol. The grid size was changed for the measurement of this object. From 4mm resolution, 2 mm resolution was obtained successfully. The reconstruction was also a success. The first image in this section is the modelled ethanol cylinder within the tank and was modelled as a dielectric cylinder with the Permittivity set to 25. All the images are sliced in the x-plane and y-plane at the centre of the object to get a complete insight of the object's dielectric values. The second image is actual ethanol cylinder reconstructed without multi-grid, i.e. with the resolution of 4 mm. The last figure is the same object reconstructed with a grid scaling from 4 mm to 2 mm. The reconstructed measurement data shows good similarity to the reconstruction of simulated data for the permittivity. This refinement in grid is a success as there is a visible amount of reduced noise in the reconstruction and will also be able to resolve Antenna with Dielectric on.

6. Conclusions and Future Work

Images for several objects were successfully reconstructed including acrylic cylinders, ethanol cylinders, vegetable oil cups and other objects, whereas for some objects the reconstruction was unsuccessful.

Grid size was successfully extended from [98 * 98 * 74] mm to [392 * 392 * 296] mm and all the antennas and cables were modelled accordingly. As the reconstruction with the extended grid was successful, now the antennas can be modelled with the dielectric on, and the performance of FDTD simulator is expected to increase by a significant factor.

Antennas in the prototype were firmly fixed by additional support from the internal side, which resulted in a better performance and stable measurements.

Permittivity is well constructed for almost all of the objects; table below gives a brief idea:

	Actual Permittivity	$\Delta\epsilon$ (Background (78) - Actual Permittivity)	Reconstructed/Converged Permittivity
Acrylic Cylinder	2.1-3.9	75	30
Vegetable Oil	3-4	74	45 (S11 Disabled)
Ethanol	25	53	67
Sugar Sol	70	8	Failed Reconstruction

Conductivity on the other hand was only successfully constructed for a metallic object. Work needs to be done in this regard to better apprehend conductivity reconstruction.

For future consideration instead of a monopole antenna with Omni-directional radiation pattern, a directive antenna should be used. Although it would be difficult to model such an antenna in the simulation domain but the results will be enhanced by orders of magnitude. Antennas employed currently are not manufactured of stainless steel and thus have rusted due to the presence of salt water in the tank.

More complex and realistic breast phantoms need to be modelled and imaged. Simulation code needs to be modified so as to reduce reconstruction time and reduce memory usage.

A dedicated server can also be allocated for this project; this will save a lot of time served in the queue waiting where several days are wasted just to get the job started.

The problem that occurred the most during the reconstruction was that the programme was either unable to converge or went unstable, saying that step goes to infinity and resulting in a large error file.

The current Analog switching matrix is also to be replaced with a faster digital switch.

Homogeneous solution of oil and water can be used as a matching liquid and the dielectric properties can be controlled by changing ratios.

Considering these suggestions it can be concluded that this system definitely has enough potential to emerge as a future tomographic system.

Bibliography

- [1] Andreas Fhager. *Microwave Tomography*. University Disseration, Chalmers University of Technology [2006]
- [2] J. H. Jacobi , L. E. Larsen and C. T. Hast "Water-immersed microwave antennas and their application to microwave interrogation of biological targets", *IEEE Trans. Microw. Theory Tech.*, vol. MTT-27, p.70 , 1979.
- [3] Mammography, Wikipedia, viewed 10 August 2011
<<http://en.wikipedia.org/wiki/Mammography>>
- [5] Sariego, J. (2010). "Breast cancer in the young patient". *The American surgeon* 76 (12): 1397–1400
- [6] World Cancer Report". International Agency for Research on Cancer. 2008. Retrieved 2011-09-26. (cancer statistics often exclude non-melanoma skin cancers such as basal cell carcinoma which though very common are rarely fatal)
- [7] Finite Difference Time Domain (FDTD), Wikipedia, viewed 10 August 2011
<http://en.wikipedia.org/wiki/Finite-difference_time-domain_method>
- [8] Kane Yee (1966). "Numerical solution of initial boundary value problems involving Maxwell's equations in isotropic media". *IEEE Transactions on Antennas and Propagation*
- [9] Cole, K.S.; Cole, R.H. (1941). "Dispersion and Absorption in Dielectrics - I Alternating Current Characteristics". *J. Chem. Phys.* 9: 341–352
- [10] Microwave Wikipedia, viewed 26 October 2011
<<http://en.wikipedia.org/microwave>>
- [11] Permittivity Wikipedia, viewed 26 October 2011
<http://en.wikipedia.org/wiki/Relative_permittivity>
- [11] Electrical Conductivity, viewed 26 October 2011
<http://en.wikipedia.org/wiki/Electrical_conductivity>
- [12] E. Polak, *Computational Methods in Optimization: A Unified Approach*. NY: Academic Press, 1971.
- [13] A. Taflove, K. R. Umashankar, B. Beker, F. Harfoush, and K. S. Yee, "Detailed FDTD analysis of electromagnetic fields" Feb. 1988
- [14] Johan Koster. *Image reconstruction and FDTD modelling for 3D microwave tomography*. Masters Thesis , Chalmers University of Technology [2011]